

# A transdimensional Bayesian method to infer the star formation history of resolved stellar populations

J. J. Walmswell<sup>1</sup>\*, J. J. Eldridge<sup>2</sup>, B. J. Brewer<sup>3</sup> and C. A. Tout<sup>1</sup>

<sup>1</sup>*Institute of Astronomy, Madingley Rd, Cambridge, CB3 0HA, UK*

<sup>2</sup>*Department of Physics, The University of Auckland, Private Bag 92019, Auckland, New Zealand*

<sup>3</sup>*Department of Statistics, The University of Auckland, Private Bag 92019, Auckland, New Zealand*

March 2013

## ABSTRACT

We propose a new method to infer the star formation histories of resolved stellar populations. With photometry one may plot observed stars on a colour-magnitude diagram (CMD) and then compare with synthetic CMDs representing different star formation histories. This has been accomplished hitherto by parametrising the model star formation history as a histogram, usually with the bin widths set by fixed increases in the logarithm of time. A best fit is then found with maximum likelihood methods and we consider the different means by which a likelihood can be calculated. We then apply Bayesian methods by parametrising the star formation history as an unknown number of Gaussian bursts with unknown parameters. This parametrisation automatically provides a smooth function of time. A Reversal Jump Markov Chain Monte Carlo method is then used to find both the most appropriate number of Gaussians, to avoid overfitting, and the posterior probability distribution of the star formation rate. We apply our method to artificial populations and to observed data. We discuss the other advantages of the method: direct comparison of different parametrisations and the ability to calculate the probability that a given star is from a given Gaussian. This allows the investigation of possible sub-populations.

## Key words:

stars: statistics - stars: formation - methods: statistical

## 1 INTRODUCTION

One of the consequences of the advances in telescopic observing power is a growing number of resolved stellar populations. These provide opportunities to investigate not only the present state of galaxies but also their pasts. If we have photometry in two or more filters then a stellar population may be conveniently represented with a colour-magnitude diagram (CMD). This yields immediate information about its history. The main-sequence (MS) turn-off, for example, indicates the brightest and hence most massive stars that are still burning core hydrogen. Because more massive stars have shorter main sequence lifetimes, the age of these stars, as predicted by stellar models, equals the time since the last episode of star formation.

It is desirable to infer the complete star formation history (SFH) of a stellar population. With detailed libraries of stellar models it is possible to produce synthetic CMDs for star formation histories that are complex functions of both metallicity and time. Distance, extinction, multiplicity and

the nature of the initial mass function (IMF) may also be considered. The large array of possible parameters means that, with the exception of especially simple systems, a subjective comparison between observed and synthetic CMDs is unhelpful. An automated process is required.

It was noted by Dolphin (1997) that the CMD of a population with a complex star formation history may be represented by the weighted sum of many *partial* CMDs, each representing a flat, constant star formation rate (SFR) over some small time interval and at a given metallicity. This is essentially an IMF-weighted isochrone that has been integrated over some small time range. The CMD of the inferred star formation history is then the linear combination of partial CMDs that provides the best fit to the observations. This is for given values of the other parameters, i.e. distance, extinction, etc. and these can then be varied to find the best overall fit.

The term ‘best fit’ encompasses a wide variety of concepts. One convenient way to compare the synthetic and the observed CMDs is by binning the data so that the observations become the number of stars per bin. The synthetic CMD is then integrated over the same bins to give

\* E-mail: jjw49@ast.cam.ac.uk

the predicted number of stars. star formation history fitting has thus traditionally been accomplished by optimising some fitting parameter that compares these bins.

With small stellar populations one either has large bins that lose too much information or small bins, most of which are empty. The problem is worse if more than two filters are available; the vast majority of the resulting multi-dimensional bins are then empty. This suggests an unbinned approach and we consider different methods for analysing unbinned data.

We also introduce a model-comparison Bayesian approach to star formation history fitting. We model the star formation history as being a series of Gaussian bursts, each with a time, width and mass. We then use Markov Chain Monte Carlo (MCMC) methods to recover the posterior probability distribution of the star formation history. We avoid the perils of overfitting by using Reversible Jump MCMC to make the number of bursts itself a variable and thus obtain the posterior probability distribution for the number of Gaussian bursts. We also show how the Reversible Jump procedure may be used to make a direct comparison between differently-parametrised models.

If we believe that the Gaussian bursts have a physical meaning, rather than being a parametrisation that happens to yield a smooth function of time, then it is of interest to know the posterior distributions of the parameters. This is made difficult by the label-switching problem. We discuss solutions to this and recommend the use of relabeling algorithms. We finally discuss how one can attempt to assign the observed stars to different bursts and how that can help identify separate populations. We apply our method to test populations and observed data.

## 2 FITTING AS PARAMETER OPTIMISATION

We begin by outlining how several different statistics have been applied to data to produce fitted model CMDs. We then explain the advantages of unbinned versus binned methods and consider two approaches by which an unbinned fitting parameter may be calculated. We conclude by raising the pitfall of overfitting.

### 2.1 Maximum likelihood with binned CMDs

Given a synthetic CMD that has been divided up into bins, the mean number of stars in the  $i$ th bin,  $m_i$ , is given by

$$m_i = \sum_j^M r_j c_{ij}, \quad (1)$$

where  $r_j$  is the contribution to the star formation history from partial CMD  $j$ , which has  $c_{ij}$  stars in bin  $i$ . There are  $M$  partial CMDs with  $N$  bins in each. This must be compared to  $n_i$ , its observed counterpart from a data set of  $S$  stars.

The method of maximum-likelihood has been widely used to fit models to data since it was popularised by R. A. Fisher in the early part of the last century. The best fit may be said to be the model that gives the highest probability of

the data given the model, the one that maximises the likelihood. This model will be a point somewhere in the space of the model parameters.

With Gaussian errors  $\sigma_{mi}$ , the probability of observing  $n_i$  stars in bin  $i$  when the model predicts  $m_i$  is

$$P_i = \sqrt{\frac{1}{2\pi\sigma_{mi}^2}} e^{-\frac{(n_i - m_i)^2}{2\sigma_{mi}^2}}. \quad (2)$$

The likelihood  $\mathcal{L}$  is then the product of these individual probabilities. They can be compared with a perfect prediction by dividing by the probability of observing  $n_i$  stars in bin  $i$  when the model predicts  $n_i$ . Multiplying all these together gives the likelihood ratio  $\mathcal{LR}$  and taking the logarithm converts the product into a sum. It may be written as

$$-2 \ln \mathcal{LR} = \sum_{i=1}^N \frac{(n_i - m_i)^2}{\sigma_{mi}^2} + \sum_{i=1}^N \ln \frac{\sigma_{mi}^2}{\sigma_{ni}^2}. \quad (3)$$

Provided that  $\sigma_{mi} = \sigma_{ni}$ , the second term vanishes and  $-2 \ln \mathcal{LR}$  is equal to the well-known  $\chi^2$  statistic. Minimising this gives the maximum-likelihood solution,

$$\chi^2 = \sum_{i=1}^N \frac{(n_i - m_i)^2}{\sigma_i^2}. \quad (4)$$

However, minimising  $\chi^2$  to find the best fit is inappropriate when fitting CMDs. As Dolphin (2002) observes, the number of stars per bin given a particular mean is a Poisson distribution.

### 2.2 Minimising $\chi_\lambda^2$

The likelihood ratio equivalent to  $\chi^2$  when the data obey Poisson statistics is  $\chi_\lambda^2$ . If there are  $m_i$  stars in the  $i$ th bin of the model CMD, compared with  $n_i$  in the comparable part of the observed CMD, the probability of the data being drawn from the model is

$$P_i = \frac{m_i^{n_i}}{e^{m_i} n_i!}. \quad (5)$$

As before this may be divided by the probability that the  $n_i$  stars would be observed when the mean is  $n_i$ . Multiplying these together gives the likelihood ratio. The natural logarithm of this when multiplied by -2 gives  $\chi_\lambda^2$ .

$$\chi_\lambda^2 = 2 \sum_i (m_i - n_i + n_i \ln \frac{n_i}{m_i}). \quad (6)$$

One can then apply a minimisation routine to find the maximum likelihood star formation history. The gradients of  $\chi_\lambda^2$  and its Hessian matrix are both simple analytic functions of the rates  $r_j$  and the partial CMDs. The latter can easily be shown to be positive-definite and hence only one minimum for  $\chi_\lambda^2$  exists. One can therefore use advanced minimisation algorithms. Dolphin (2002) used the Fletcher-Reeves-Polak-Ribiere (FRPR) algorithm (Press et al. 1992), which proceeds by performing a series of line minimisations. His method has been widely used since then (Weisz et al. 2011).

### 2.3 Minimising $\chi_\gamma^2$

Mighell (1999) proposed instead a new statistic  $\chi_\gamma^2$  which both minimises properly and is more  $\chi^2$ -like in form.

$$\chi_\gamma^2 = \sum_{i=1}^N \frac{(n_i + \min(n_i, 1) - m_i)^2}{n_i + 1} \quad (7)$$

It should be noted that  $\chi_\gamma^2$  only in the limit of many data points minimises to the maximum-likelihood means of Poisson data (Hauschild & Jentschel 2001). This statistic has been used to deduce star formation histories, most notably by Aparicio & Hidalgo (2009) who use a genetic algorithm to minimise it and have made their code available on the Internet<sup>1</sup>.

#### 2.4 The unbinned likelihood: Method 1

Binning methods are problematic if too few stars have been observed. So little information is then available that it is unwise to throw any of it away by using large bins. However a fine binning scheme results in many empty bins or bins containing but a single star. A similar problem emerges if we have observations in more than two filters. In principle this should be desirable because more data is then available to constrain the star formation history. However the data and the model are then more than two-dimensional and, by the curse of dimensionality, most bins are again empty, even if the data set is large.

The classical unbinned maximum-likelihood method (Jegerlehner et al. 1996) considers the limit of the Poisson likelihood as the bins become very small so that each bin contains either one star or zero stars. As before,  $N$  is the number of bins and  $S$  is the number of observed stars. This definition of the likelihood can be written as

$$\mathcal{L}_1 = \prod_{i=1}^N \frac{m_i^{n_i}}{e^{m_i} n_i!}, \quad (8)$$

and separating out the product over the bins with one star and with zero stars gives

$$\mathcal{L}_1 = \prod_{i=1}^S m_i e^{-m_i} \prod_{i=1}^{N-S} e^{-m_i}. \quad (9)$$

If we combine the products of  $e^{-m_i}$  we get

$$\mathcal{L}_1 = \prod_{i=1}^S m_i \prod_{i=1}^N e^{-m_i}. \quad (10)$$

The Poisson mean per bin  $m_i$ , can be taken to be  $p(x, y) dx dy$ , i.e. we introduce a probability density function  $p(x, y)$  that depends on position within the CMD. The second product is over the entire CMD. It becomes the exponential of the sum over  $m_i$ , which in turn is equivalent to integrating the CMD. If the  $i$ th star is at  $x_i, y_i$  we have

$$\mathcal{L}_1 = \prod_{i=1}^S p(x_i, y_i) [(dx dy)^S e^{-\int p(x, y) dx dy}]. \quad (11)$$

Providing that  $p(x, y)$  has a fixed normalisation, the factor in the square brackets will be constant. The likelihood is then proportional to the product of the values of  $p(x, y)$  at the location of the observed stars.

$$\mathcal{L}_1 \propto \prod_{i=1}^S p(x_i, y_i). \quad (12)$$

The obvious normalisation of  $p(x, y)$  is so that it integrates to one. For consistency one should perform the integration over a fixed area in apparent magnitude and uncorrected colour, within which the data points are fixed locations. It is thus always the probability density function of observing a star given the model. Varying the star formation history, the distance or the extinction will alter  $p(x, y)$  and so it must be re-normalised.

So far we have not discussed how to deal with errors. To compare with the data we need the model CMD after it has undergone the same error processes involved in the observations. It then becomes the probability density function of obtaining the observed photometry. We thus consider  $\rho(x, y)$ , the probability density function of the pure model CMD, that is, of a star having certain photometry and  $p(x, y)$ , the probability density function of the model with errors, that is, of a star being observed to have certain photometry. The probability of observing the  $i$ th star,  $p_i = p(x_i, y_i)$  is

$$p_i = \int \rho(x_0, y_0) U(x_i - x_0, y_i - y_0) dx_0 dy_0, \quad (13)$$

where  $U(x_i - x_0, y_i - y_0)$  is an error function that varies with position in the CMD. It has the effect of taking each point in  $\rho(x_0, y_0)$  and spreading it over an error kernel. The natural choice is a Gaussian:

$$U(x_i - x_0, y_i - y_0) = \frac{1}{2\pi\sigma_x\sigma_y} e^{-\frac{(x_i - x_0)^2}{2\sigma_x^2}} e^{-\frac{(y_i - y_0)^2}{2\sigma_y^2}}, \quad (14)$$

where  $\sigma_x(x_0, y_0)$  and  $\sigma_y(x_0, y_0)$  are the errors as a function of position within the CMD. The easiest way to define the errors is to partition the CMD into a Voronoi Tessellation: each point adopts the errors of the nearest observation. A better method would be to analyse the response of the observing apparatus and the reduction method to artificial stars. We have so far ignored the other principal source of deviation from an ideal situation: incompleteness at dimmer magnitudes. If the form of the completeness function is known then it can be applied to  $\rho(x, y)$  before the error-blurring process.

Whether one is interested in maximising the likelihood or applying Bayesian methods it will be necessary to calculate this likelihood repeatedly for different star formation rates. It is thus desirable to minimise the computational load. The error process can be applied to the pure partial CMDs at the beginning of the analysis. These partial CMDs must not be normalised individually: the fact that older populations have fewer stars is important information, it means that the more massive entities have died. Instead one can record two sets of data:  $p_{ij}$ , the value of the  $j$ th partial CMD at the location of the  $i$ th observed star; and  $N_j$ , the value obtained by integrating the  $j$ th CMD over the allowed range of colour and magnitude. The arrays that define the partial CMDs can then be ignored and the likelihood becomes

$$\mathcal{L}_1 \propto \prod_{i=1}^S \frac{\sum_{j=1}^M r_j p_{ij}}{\sum_{j=1}^M r_j N_j}. \quad (15)$$

where  $r_j$  is the star formation rate associated with the  $j$ th blurred CMD. These must sum to one and the denominator

<sup>1</sup> <http://iac-star.iac.es/iac-pop>

in the fraction is required to normalise each probability. If the distance and/or extinction are varied then the positions of the model stars will shift and the  $p_{ij}$  will thus be different. The normalisation factors will also change.

## 2.5 The unbinned likelihood: Method 2

Unfortunately it is not always reasonable to assume a universal error function. We may have two stars in a similar part of the CMD but with different photometric errors, a result perhaps of different observing conditions. The stars may also be so few that we cannot obtain reasonable error coverage of the CMD. Under such circumstances it seems natural to calculate the probability of each star given the model by integrating  $\rho(x, y)$  with an error function that represents the observational uncertainties. This approach goes back to Tolstoy & Saha (1996), who approximated their model CMD by drawing from it an equal number of stars to that in the dataset. Their method had the disadvantage of introducing unnecessary randomness: the same model CMD will produce different model populations. Naylor & Jeffries (2006) improved the method by instead comparing the data directly with the model CMDs. They defined the probability of making the  $i$ th observation to be

$$p_i = \int \rho(x_0, y_0) U_i(x_0 - x_i, y_0 - y_i) dx_0 dy_0, \quad (16)$$

where  $U_i(x_0 - x_i, y_0 - y_i)$  is the error function of the observation. They defined the statistic  $\tau^2$  by analogy with  $\chi^2$  so that

$$\tau^2 = -2 \ln \prod_{i=1}^S p_i = -2 \sum \ln p_i, \quad (17)$$

and minimised it to find the distances and ages of open clusters. This approach defines  $\mathcal{L}_2$ , the second definition of the likelihood.

$$\mathcal{L}_2 = \prod_{i=1}^S \int \rho(x_0, y_0) U_i(x_0 - x_i, y_0 - y_i) dx_0 dy_0. \quad (18)$$

If we take the error function to be a Gaussian we have

$$U(x_0 - x_i, y_0 - y_i) = \frac{1}{2\pi\sigma_{x,i}\sigma_{y,i}} e^{-\frac{(x_0-x_i)^2}{2\sigma_{x,i}^2}} e^{-\frac{(y_0-y_i)^2}{2\sigma_{y,i}^2}}, \quad (19)$$

where the star is at  $x_i, y_i$  and has associated errors  $\sigma_{x,i}$  and  $\sigma_{y,i}$ . This looks very similar to Equation 14 but is crucially different: with  $\mathcal{L}_1$ , to find the probability of a single observation we required the errors as a function of position to determine how different points in  $\rho(x, y)$  could be scattered into  $p(x, y)$ . To find the probability of a single observation with  $\mathcal{L}_2$  we use its errors alone. The two definitions will be the same if the errors are everywhere constant and this is true more generally for invariant error functions that are symmetric about the observations. In practice they will give similar results if the errors change over a longer length-scale than the model. If the errors become very small then the Gaussians become delta-functions. Both definitions of the probability of an observation then reduce to the value of  $\rho(x, y)$  at the location of the observation.

The appropriate normalisations for  $\rho(x, y)$  and  $U_i(x_i - x_0, y_i - y_0)$  require some thought. Naylor & Jeffries (2006)

normalised the error functions so that they had the same maximum value, with the aim of recovering  $\tau^2 = \chi^2$  when the model is a curve and the uncertainties are only in one dimension. However, an alternative choice, proposed by Naylor (2009), is that both the model and the error functions integrate to one. This is the normalisation that we adopt. This decision may be put on more rigorous footing by noting that it is equivalent to treating them as probability distributions that represent different types of uncertainty. The distribution  $\rho(x, y)$  represents the random uncertainty resulting from a drawing from the model. By contrast,  $U_i(x_i - x_0, y_i - y_0)$  represents the epistemic uncertainty due to imprecise data. In the terminology of Denoeux (2013) it is a Bayesian belief function. The likelihood may then be considered to be the probability of *fuzzy* data given the model. As with  $p(x, y)$ ,  $\rho(x, y)$  must be normalised over a fixed area in apparent magnitude and uncorrected colour.

For it to be possible to multiply them together it is necessary that the belief functions be defined over the same domain as the model. This may not always be the case. One often has reasons to impose a cut in apparent magnitude. This may be to obtain a sample with a high and constant completeness and thus to avoid the consideration of completeness functions. In addition, dimmer stars not only often have greater photometric errors than their more massive and brighter brethren but their long lifetimes make them poor tools for age determination. One of the outcomes of this cut will be a number of stars that have non-trivial parts of their belief functions outside the region specified by the model. Possible responses are to either drop these stars from the sample or to perform the integration over only the area of the CMD allowed by the cuts. We adopt the latter approach but note that it is not, strictly speaking, correct. One can imagine the case of a star that, thanks to errors, is above the magnitude cut, though the area of the model CMD that best matches it is below. In practice we do not find that this causes problems when we consider synthetic populations in a later section.

A method for maximising something akin to  $\mathcal{L}_2$  in the context of the inference of star formation histories was proposed by Small et al. (2013). The principal difference is that they calculate the probability of observing each star given the model by *separately* multiplying each isochrone, as considered in a magnitude-magnitude diagram, with a completeness function and the IMF and then integrate with the Gaussian error functions. The analogous approach with our method is to integrate each un-normalised partial CMD  $\rho_j(x, y)$  with each error function  $U_i(x_i - x_0, y_i - y_0)$  to get  $q_{ij}$ . The probability of an observation is then the normalised weighted sum of these, with the weights given by the rates  $r_j$ . The likelihood then becomes

$$\mathcal{L}_2 \propto \prod_{i=1}^S \frac{\sum_{j=1}^M r_j q_{ij}}{\sum_{j=1}^M r_j N_j}, \quad (20)$$

where, as at the end of Section 2.4,  $N_j$  is the value obtained by integrating the  $j$ th partial CMD over the allowed range of colour and magnitude. The advantage of this approach is that one can then calculate the likelihood for different rates much quicker than if one had to repeatedly integrate over the CMD.

The second definition of the likelihood,  $\mathcal{L}_2$ , is always going to be preferable when one cannot use an overall error function, although, as we have noted, it may become problematic if cuts are imposed. We use  $\mathcal{L}_2$  in the later sections but briefly contrast it with  $\mathcal{L}_1$  when we consider real data.

## 2.6 Overfitting and the choice of temporal bins

When constructing the partial CMDs we must pick a temporal binning scheme. The bin boundaries are nearly always chosen to be fixed advances in the logarithm of time (Dolphin 2002). This is to reflect the decreasing degree by which stellar populations change over time: massive stars evolve faster and die younger.

We might think that we ought to bin in time as finely as possible so as to recover all the detail in the star formation history. This is encouraged by the fact that the maximised likelihood increases monotonically with the number of bins. This is a more general result: the maximum likelihood increases with model complexity. Eventually though the model would be fitting random variations in the data. Overfitting would have occurred and this is wasteful at best and misleading at worst.

With partial CMDs there is a particular problem in that, as the time-bin size decreases, adjacent CMDs become more and more similar. The errors on the rates become increasingly correlated and the likelihood surface becomes flat. This means that the rates can be altered considerably without affecting the fitting parameter. The estimates for the rates are then effectively meaningless. A typical phenomenon is that, of two adjacent partial CMDs, one is a slightly better fit to the data. The other rate is then set to zero and the star formation history takes on an unpleasant jagged form. This phenomenon may be verified by fitting, for example, the first fifty or so prime numbers with  $Ax + Bx^{1.00001}$  in Mathematica. With no constraints, A and B have very large values and opposite signs. When zero values are prevented one is positive and the other zero.

To prevent overfitting we require some sort of application of Occam's Razor: the simplest (good) explanation is the best. Within the maximum-likelihood framework we may apply three methods. First, picking a fitting and a testing set from the data and applying the methods of bootstrapping or cross-validation. Secondly there are several information criteria that penalise models with more parameters. The original of these is the Akaike Information Criterion (Akaike 1974) or AIC.

$$\text{AIC} = -2\ln(\mathcal{L}) + 2M. \quad (21)$$

Instead of maximising the likelihood we minimise the AIC. The solution is the model that minimises the expected information loss in the asymptotic limit. It is thus poorly adapted to small data sets. An alternative is the Bayesian Information Criterion (BIC) of Schwarz (1978),

$$\text{BIC} = -2\ln(\mathcal{L}) + M\ln(N), \quad (22)$$

where  $N$  is the number of data points, CMD bins in the binned case, observed stars in the unbinned case, and  $M$  is the number of parameters.

The third method is regularisation, that is, the penalising of models where the output is not smooth. Jørgensen & Lindegren (2005a) considered the likelihood of

a data set given a star formation rate based on very narrow time bins and maximised it with the aid of a smoothing parameter  $\alpha$ . The problem with this approach is that the choice of smoothing parameter is non-trivial and ad hoc, it is as arbitrary as the problem of choosing the appropriate number of bins. The errors on the rates are also then difficult to calculate.

## 3 FITTING AS BAYESIAN INFERENCE

We propose a new method. We start by noting that the likelihood is the probability of the data given the model, whereas the probability of the model given the data is what is really desired. We thus consider Bayes' Theorem: instead of just considering the likelihood we combine it with the prior probability distribution to get the posterior probability distribution. For parameters  $\theta$ , data  $D$  and model  $M$ , that is, the parametrisation, we have

$$\Pr(\theta | D, M) = \frac{\Pr(D | \theta, M) \Pr(\theta | M)}{\Pr(D | M)}. \quad (23)$$

More generally, for model fitting we have

$$\text{Posterior} = \frac{\text{Likelihood} \times \text{Prior}}{\text{Evidence}}. \quad (24)$$

The aim is to infer the posterior, which is a *probability distribution* rather than a point estimate. It represents the belief of a reasonable person, given both their prior beliefs and the information provided by the data. This natural interpretation, that model inference is a problem in probability theory, is the best justification for the Bayesian approach.

It should be noted that more-or-less Bayesian methods have been applied to colour-magnitude problems before. Tolstoy & Saha (1996) described their fitting method as Bayesian but given that it consists of maximising the posterior given flat priors it is entirely equivalent to maximising the likelihood. Jørgensen & Lindegren (2005b) considered open clusters and calculated the posterior probability of the age of each star given its photometry. Their method is also not fully Bayesian: instead of considering the full posterior distribution they derive confidence intervals based on analogies with  $\chi^2$ . Finally, von Hippel et al. (2006) presented a fully Bayesian method for inferring the posterior distributions of the masses of stars within a cluster and the cluster parameters (age, distance, metallicity and extinction). This is a similar but different problem: they assumed a coeval population and solved for the masses, we assume a common mass function and solve for the star formation history.

In the remaining part of this section we describe our parametrisation, consider appropriate priors, and discuss how best to represent the posterior. We then show how Bayesian methods allow us to avoid overfitting.

### 3.1 The parametrisation

Star formation in clusters is often observed to have occurred in bursts (Kauffmann et al. 2003), the result perhaps of collisions with gas clouds or other clusters. More generally we expect a star formation history to exhibit a degree of temporal correlation: if we know the rate at a particular time then we do not expect it to change drastically over some

small interval. This inspires us to propose a model whereby the star formation history is represented as a number  $M$  of Gaussians in linear time, each with parameters  $\theta_i$ : time before the present day (mean)  $t_i$ , width (standard deviation)  $w_i$ , and mass  $\pi_i$ .

$$r(t) = \sum_{i=1}^M \pi_i \mathcal{N}(t; t_i, w_i^2). \quad (25)$$

Our use of the unbinned likelihood means that the model CMD is then the probability density function of observing one star. This means that the masses assigned to each Gaussian are merely relative weights and can be considered to sum to one. The model CMD is produced by first generating  $B$  partial CMDs by binning the models in linear time on a sufficiently small timescale. We used 1 Myr. The linear combination is then formed as before with the weights given by the function  $r(t)$ .

### 3.2 The prior probabilities

By default we have no a priori reason to suspect any time is more likely to have a burst than any other, with the obvious caveat that the burst time cannot be later than the present day or earlier than the age of the universe. We thus adopt a uniform prior on  $t_i$  over this range.

The widths are scale parameters and to represent our uncertainty concerning them is more difficult. This becomes apparent as soon as alternative parametrisations are considered: we could have used the variance  $w_i^2$  or the precision  $w_i^{-1}$  as measures of the width of a burst. Using a uniform prior with one parameter is then equivalent to using a non-uniform prior with the others. Different parametrisations will give different results. We therefore adopt the Jeffreys prior (Jeffreys 1946), which is constructed so that it has the desirable property of being invariant under reparametrisation. For a vector of parameters  $\theta$ , the Jeffreys prior is

$$\Pr(\theta) \propto \sqrt{|\mathbf{I}(\theta)|}, \quad (26)$$

where  $|\mathbf{I}(\theta)|$  is the determinant of the Fisher information matrix. The Jeffreys prior for the standard deviation of a Gaussian is  $\Pr(w_i) \propto 1/w_i$ . This inverse prior represents the fact that we are ignorant as to the *scale* of the parameter and is equivalent to assuming a uniform distribution in log time (see Section 3.1 in Jeffreys (1939) for the argument that the prior for a semi-infinite parameter should be its reciprocal). We do however impose a lower limit of 1 Myr on  $w_i$ .

For the masses we use the symmetric Dirichlet distribution with concentration parameter  $\alpha$ . It represents the probability of obtaining a set of masses on the simplex  $\sum \pi_i = 1$  when no component is favoured over another.

$$\Pr(\pi | M) = \frac{\Gamma(\alpha M)}{\Gamma(\alpha)^M} \prod_{i=1}^M \pi_i^{\alpha-1}. \quad (27)$$

The parameter  $\alpha$  represents the degree to which we expect the masses to differ. If  $\alpha > 1$  we favour distributions where the masses are similar whereas if  $\alpha < 1$  we suspect that sparse distributions are more likely. We adopt  $\alpha = 1$ . We note that  $\alpha = 0.5$  is the Jeffreys prior but find that we get almost identical solutions.

### 3.3 The posterior probabilities of the star formation history

Once we have determined the form of the posterior distribution we then sample it with Markov Chain Monte Carlo (MCMC) methods. A simple Metropolis-Hastings (Hastings 1970) algorithm is adequate for this task. The algorithm is initiated with a randomly-chosen set of model parameters, that is, at a random location in the space defined by the model parameters. A new, nearby location is then proposed based on a random jump drawn from a proposal distribution. The ratio of the posterior probabilities are then compared. If the new location is more probable than the current location then the new location is adopted and the corresponding model parameters are recorded. If the new location is less probable then it is likewise adopted but with a probability equal to the posterior ratio. If the new location is not adopted then the model parameters of the current location are recorded once more.

After initialisation the algorithm moves towards the location of the bulk of the probability. This process is known as burn-in and the parameter values in this stage are dependent on the starting-position and must be ignored. Once the algorithm has reached the location of the bulk of the probability it wanders about this subset of the parameter space. In doing so it recovers an increasingly-accurate estimate of the posterior probability distribution. The algorithm may be said to have converged when the output posterior is the same, to a chosen degree of precision, for different starting locations.

The evaluation of the posterior probability at a particular set of parameters requires, for the blurred likelihood  $\mathcal{L}_1$ , the  $SB$  relative probabilities that correspond to the value of the  $B$  blurred partial CMDs at the location of the  $S$  stars, and the function  $r(t)$ . The integrated likelihood  $\mathcal{L}_2$ , which is the one we principally use, requires the  $SB$  relative probabilities corresponding to the integration of the  $S$  stellar error functions with the  $B$  pure partial CMDs, and the function  $r(t)$ . Only  $r(t)$  must be recalculated each time for either method and thus the algorithm can accumulate enough samples for good convergence very quickly. This is not altered by the addition of more filters. The principal effect of fitting a higher-dimensional structure that involves more than two filters is that generating the models becomes a lengthier process.

The posterior distribution of the star formation history has  $3M$  dimensions and is difficult to represent. One approach is to take several random drawings from the distribution. This gives some idea of the probable nature of the star formation history and its variability but does not incorporate all the information provided by the posterior. The approach we take is to determine the posterior distribution of the rate  $r(t)$  by recording the rate at each point on the Markov Chain. The mean rate at a particular time is then easily calculated. To find the uncertainties we reflect that, in Bayesian terms, they define a credible interval in which we believe that the rate has a certain probability of being. The more compact the interval the more informative it is. We thus adopt the mode as our best estimate of the rate and then construct the lower and upper limits about it such that they form the most compact interval in which the rate has a 68 per cent chance of being. This is an arbitrary num-

ber but allows an intuitive connection with the idea of  $1\sigma$  error bars. If the posterior distributions of the rates are reasonably normal in appearance then this approach offers an adequate representation.

### 3.4 The posterior probabilities of the parameters

It is important to note that the labelling of the Gaussians is not in itself intrinsically important to the inferred star formation history. The likelihood is invariant under label-switching. This causes the posterior distribution to have  $M!$  identical modes. The probability density function for each parameter can be found by summing the full posterior distribution over the other parameters. This process is known as marginalisation and assuming full convergence, each parameter of the same type has the same marginal distribution.

The Gaussian burst parametrisation may be no more than a convenient way of generating a temporally-correlated star formation history. If however we believe that we have identified individual bursts then it may be of interest to know their parameters. There are several methods by which this may be attempted (Jasra et al. 2005). The easiest way is to process the MCMC output to reorder the bursts by time to impose an artificial identifiability constraint. The marginal probabilities for a certain burst’s parameters are then those of the burst that has a certain relative position given the presence of the others. We find that this generally offers only a limited solution and that the posterior marginal distributions are still multimodal. It is easy, for example, to conceive of a scenario where one pair of bursts might be best distinguished by their times and another, with similar times, by their widths or masses.

Another method, proposed by Marin et al. (2005), is to make use of the set of parameters in the MCMC output that gave the highest posterior probability. This is the maximum a posteriori (MAP) set of parameters and is the Bayesian analogue of the maximum-likelihood solution. It is usually an extreme case and may be unrepresentative of the location of the bulk of the probability. For this reason we generally do not use it when considering the overall star formation history. Nevertheless it provides a standard by which the other samples can be compared. Marin et al. (2005) suggest that one should relabel the MCMC output so that each sample resembles the MAP estimate as much as possible according to some chosen distance metric. We do not find that this method removes the symmetry from the posterior distributions any better than an identifiability constraint.

We instead adopt the iterative relabeling algorithm approach of Stephens (2000b). In this, one first identifies a loss function based on the MCMC output. One then relabels each sample to minimise the loss function and repeats until convergence. We start from the premise that, if the number of bursts has good posterior support, there should exist a permutation of the MCMC outputs such that the posterior distribution of each parameter is reasonably close to a normal distribution. We first calculate the mean  $\mu_i$  and variance  $\sigma_i^2$  of the parameters given the current set of orderings. We then permute each MCMC sample such that the product of the values of the normal distribution with these means and variances and at each parameter value is minimised. This is the loss function

$$\mathcal{L}_0 = -\log\left(\prod_{i=1}^{3M} \mathcal{N}(\theta_i; \mu_i, \sigma_i^2)\right), \quad (28)$$

where the product is over the  $3M$  model parameters: the times, widths and masses of the  $M$  bursts. We recalculate the new means and variances and repeat. This algorithm converges on the relabelling scheme that yields the most normal-like form of the posterior distributions given the starting point. A global optimum can be ensured by running the algorithm repeatedly from a number of different starting points and taking the output that gives the most normal-like behaviour overall.

We find that this approach usually removes the symmetry from the posterior distributions and that any multimodality can then be considered as evidence for an alternative model. We note that the full marginal distributions are not conveniently presented and that it is helpful to reduce them to point estimates and uncertainties. Modes and credible intervals usually suffice.

### 3.5 The classification probabilities

Another consequence of a belief that the bursts are physically meaningful is a desire to ascertain which stars belong to which burst. This can be accomplished by reporting  $\mathbf{U}$ , the matrix of the classification probabilities of star  $i$  being due to burst  $j$ . The matrix  $\mathbf{U}$  may be estimated from the MCMC output by considering  $\mathbf{V}(\boldsymbol{\theta})$ , the classification probabilities given a set of parameters  $\boldsymbol{\theta}$  from an MCMC sample. The unbinned likelihood of obtaining star  $i$  from burst  $j$  is  $f_i(\boldsymbol{\theta}_j)$ .

$$V_{ij}(\boldsymbol{\theta}) = \frac{f_i(\boldsymbol{\theta}_j)}{\sum_{l=1}^M f_i(\boldsymbol{\theta}_l)}. \quad (29)$$

The matrix  $\mathbf{U}$  is then given by

$$U_{ij} = \frac{1}{R} \sum_{s=1}^S V_{ij}(\boldsymbol{\theta}_s), \quad (30)$$

where there are  $R$  MCMC samples. We calculate the classification probabilities for each star and assign them to the most probable burst if this probability is greater than 0.75. Otherwise their origin is considered to be unclear and they are labelled accordingly.

### 3.6 Model comparison

Instead of the number of temporal bins, the choice of model now becomes the number of bursts. We are unlikely to know a priori the appropriate number of bursts and so the best set of parameters may be said to be ‘unknown unknowns’: we don’t know their values and don’t know that we ought to. This Rumsfeldian<sup>1</sup> problem may be addressed by considering the joint posterior probability of both the model index ( $M$ , the number of bursts) and the parameters  $\boldsymbol{\theta}$ ,

<sup>1</sup> “There are known knowns; there are things we know we know. We also know there are known unknowns; that is to say, we know there are some things we do not know. But there are also unknown unknowns - the ones we don’t know we don’t know.” Donald Rumsfeld, US Secretary of Defense, 12th February 2002.

$$\Pr(M, \boldsymbol{\theta} | D) \propto \Pr(M) \Pr(\boldsymbol{\theta} | M) \Pr(D | M, \boldsymbol{\theta}). \quad (31)$$

$\Pr(\boldsymbol{\theta} | M)$  is the prior probability of the parameters and  $\Pr(D | M, \boldsymbol{\theta})$  is the likelihood. The model prior  $\Pr(M)$  represents our opinion as to how probable different numbers of bursts are. If we think that the number of bursts could be anywhere between one and infinity then there is an argument for using  $\Pr(M) \propto 1/M$  in the same spirit as the Jeffreys prior on the widths. This level of prior ignorance is not really applicable here. The aim of this process is primarily to find the minimum number of bursts that will represent the data properly: any more would be effectively superfluous and would merely model random error. Each burst represents three additional parameters and, for populations of hundreds to thousands of stars, it would be unreasonable to use more than a few dozen parameters for modelling purposes.

We therefore follow Richardson & Green (1997) in adopting a uniform prior between  $M = 1$  and  $M = M_{\max}$ , with  $M_{\max}$  chosen with the assumption that the posterior probability associated with it will be low. If this is not the case then the analysis is repeated with a higher value.

The joint posterior may be factorised as

$$\Pr(M, \boldsymbol{\theta} | D) \propto \Pr(M | D) \Pr(\boldsymbol{\theta} | M, D). \quad (32)$$

The first probability,  $\Pr(M | D)$ , is the posterior probability of the model. The second is the more familiar posterior probability of the parameters given the model. This means that, given the joint posterior, we can marginalise over the parameter values to find the model posterior. We can then pick the model with the greatest posterior probability and use its probability distribution for the parameters.

The Reversible Jump MCMC method of Green (1995) offers a way to recover the joint posterior. The essence of the method is to consider the Metropolis-Hastings proposals to be on a space that includes model variability and to adjust the acceptance ratios accordingly. We thus use the following simple method based on the work of Stephens (2000a). The Markov chain is able to perform three moves: an ordinary shift move within the current model, a birth move that adds a new Gaussian, its parameters drawn from the prior, and a death move, in which a random Gaussian is removed. Because the masses are obliged to sum to one, a transdimensional move will affect them all; the other parameters are not affected. We have, for a birth move that adds a new burst with a mass of  $\pi_{(M+1)}^{(M+1)}$ ,

$$\pi_{(i)}^{(M+1)} = \pi_{(i)}^{(M)} (1 - \pi_{(M+1)}^{(M+1)}), \quad (33)$$

where the superscript indicates the total number of bursts and the subscript the burst number. A death move similarly rescales the masses of the surviving bursts. For ordinary Metropolis-Hastings moves within a fixed model the acceptance ratio  $a$  is

$$a(x, y) = \min \left( 1, \frac{P(x)Q(x|y)}{P(y)Q(y|x)} \right), \quad (34)$$

where  $x$  and  $y$  represent two locations in the parameter space,  $P$  the posterior probability and  $Q$  the proposal distribution. In the transdimensional setting and for the case of moving between a model with one parameter to one with two this becomes

$$a_{12} = \min \left( 1, \frac{P(2, (\theta_1, \theta_2))c_{21}}{P(1, \theta)q(u)c_{21}} \left| \frac{\partial(\theta_1, \theta_2)}{\partial(\theta, u)} \right| \right). \quad (35)$$

The variables  $c_{12}$  and  $c_{21}$  are the probability of proposing the forward and reverse moves respectively. Note that if we move from  $M$  to  $M + 1$  bursts, the probability of moving back to the original state is the death rate multiplied by  $1/(M + 1)$ . The one-parameter state had value  $\theta$ , to which we apply the random variable  $u$  to get the new state  $\theta_1, \theta_2$ . The prior probability of  $u$  is  $q(u)$ . The final element is the Jacobian of the transformation. With our model the masses of the bursts are the only original variable that is changed and this only depends on the new mass. The Jacobian thus becomes  $(1 - \pi_{(M+1)}^{(M+1)})^M$  and the acceptance ratio for a birth is

$$a_{\text{birth}} = \min \left( 1, \frac{P_{\text{new}}(d/(M+1)) (1 - \pi_{(M+1)}^{(M+1)})^M}{P_{\text{old}} Q b} \right), \quad (36)$$

where  $Q$  is the joint prior on the parameters of the new burst,  $P_{\text{old}}$  is the posterior probability of the old state with  $M$  bursts and  $P_{\text{new}}$  that of the new state with  $M + 1$  bursts. The quantities  $b$  and  $d$  are the probabilities of the algorithm proposing a birth or death move. The acceptance ratio for a death move is the inverse of this expression, with the difference that the prior  $Q$  is that of the burst that is to be removed.

With this transdimensional Metropolis-Hastings method we can recover the joint model posterior over the parameters and the model index. More complicated models are automatically penalised by this process because the prior becomes spread over more dimensions. The prior probability of a given set of parameters is then reduced, even though the likelihood will be greater. The algorithm thus applies Occam's Razor and ends up with the minimum number of bursts required to explain the data.

We can also make direct comparison between models of different types: all that is required is a jump move and an associated Jacobian. It was suggested to us that exponentials might be a better way of representing the star formation history than Gaussians. This is not unreasonable: there is no particular reason to expect a burst to be symmetrical.

We tested this by adding a fourth type of Metropolis-Hastings move, model switching between Gaussians and exponentials. We identified the mass, mean time and width of the Gaussians with the mass, start time and time constant of the exponentials. This transformation has a Jacobian of 1 and, as we used the same Jeffrey's priors, the acceptance probabilities are just the ratio of the posterior probabilities. We found that, for the observed data that we considered, the Gaussians received about three times more posterior support than the exponentials. This justifies their use. We note in passing that jumps between different models can suffer from poor acceptance rates, particularly if the models are very different. If this is the case then we recommend the use of Diffusive Nested Sampling (Brewer et al. 2011).

A final point is that, as Richardson & Green (1997) observed, model switching greatly assists the mixing of the Markov chain within a particular model. The random addition and subtraction of Gaussians means the chain is able to traverse the posterior landscape in jumps and is much less likely to get stuck around a single mode.

#### 4 THE STELLAR MODELS

Our synthetic partial CMDs were produced with output from the Cambridge STARS code. This was originally developed by Peter Eggleton in the 1960s (Eggleton 1971). It uses a non-Lagrangian mesh, where the mesh function ensures that the points are distributed so that quantities of physical interest do not vary by a large amount in the intervals. The code has been gradually improved and updated and the work in this paper is based on the code described by Stancliffe & Eldridge (2009) and references therein.

Convection is included in the code via the mixing length theory of Böhm-Vitense (1958) with a solar-calibrated mixing length parameter of  $\alpha = 2.0$ . We use the mass-loss scheme described by Eldridge et al. (2008). For main-sequence OB stars the mass-loss rates are calculated according to Vink et al. (2001) and for all other non-Wolf-Rayet stars we use the rates of de Jager et al. (1988), where the metallicity fraction by mass ( $Z$ ) scaling goes as  $(Z/Z_{\odot})^{0.5}$ . This theory is older but the rates have been recently tested for red supergiants and been shown to be still the least-worst available (Mauron & Josselin 2011). We use the rates of Nugis & Lamers (2000) for Wolf-Rayet stars but scale them according to metallicity again by  $(Z/Z_{\odot})^{0.5}$ . The value of the Wolf-Rayet scaling exponent is somewhat uncertain but some degree of scaling is required to give better agreement with observations (Eldridge & Vink 2006).

We created a library of evolution models with different values of  $Z$ . The fractions of hydrogen and helium were determined on the assumption of constant helium enrichment from the primordial condition of  $X=0.75$ ,  $Y=0.25$ . We then calibrated to a Solar composition of  $X=0.70$ ,  $Y=0.28$  and  $Z=0.02$  so that  $Y = 0.25 + 1.5Z$ . The masses start at  $0.5 M_{\odot}$  and increase every  $0.1 M_{\odot}$  to  $3 M_{\odot}$ , every  $0.2 M_{\odot}$  to  $12 M_{\odot}$ , every  $0.5 M_{\odot}$  to  $20 M_{\odot}$ , every  $1 M_{\odot}$  to  $50 M_{\odot}$  and every  $2 M_{\odot}$  to  $100 M_{\odot}$ .

These models were processed to generate observed magnitudes with the BaSeL V3.1 model atmosphere grid (Westera et al. 2002) and the relevant broad-band filter functions. The magnitudes were then interpolated for the values at different fractions through the life of the stars and these were then in turn interpolated between the masses. This meant that interpolation in mass was between models at equivalent stages in their lives. The relevant parts of each interpolated stellar evolution track were then assigned to the appropriate time bin with a weighting set by the model timestep and the IMF.

#### 5 APPLICATION TO SYNTHETIC POPULATIONS

We began by testing our method with synthetic populations with a known star formation history. We used  $Z=0.008$  for the metallicity, principally because we use the same models in the following section when we consider real data. These observations were in F435W, F555W and F814W, which for brevity we refer to as B, V and I, although at no point did we actually convert to the Johnson-Cousins filters. We ran the Markov Chain until six million samples were obtained and discarded the first 50,000 of these to avoid the burn-in phase. The posterior distributions were tested for consistency by running the program repeatedly from different

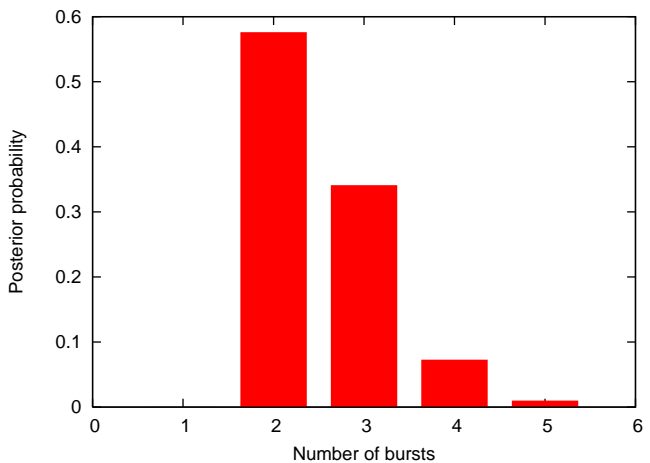


**Figure 1.** The posterior probabilities of the number of bursts used to fit Population 1. Two bursts give the best fit.

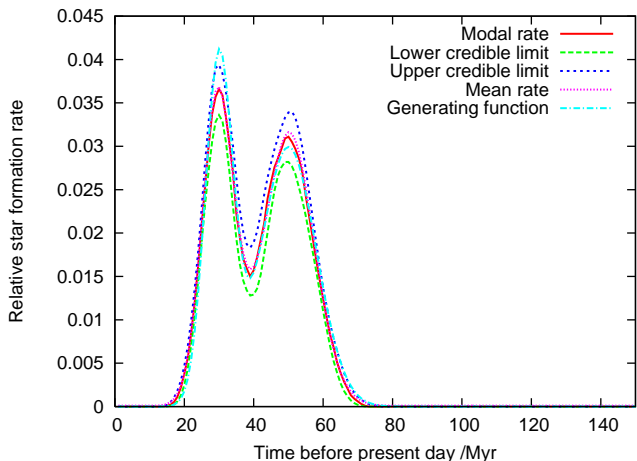


**Figure 2.** The inferred star formation history of Population 1. The posterior probability of the star formation rate at each point in time is summarised by its mean, mode and minimum 68 per cent credible interval. The generating function is the star formation history from which the test population was produced.

starting points. The probability of a birth move was set to 0.2, a death move to 0.2 and a shift move to 0.6.

##### 5.1 Population 1: Two Gaussian bursts

The least demanding test is to see whether the program can fit a stellar population that is genuinely composed of Gaussian bursts. We considered a simple star formation history consisting of two bursts and the parameters we chose are listed in Table 1. We formed the synthetic CMD in  $V$  from  $-3$  to  $-8$  and in  $V - I$  from  $-1$  to  $-3$  and applied a simple but somewhat arbitrary error function that depended inversely on magnitude. The error in the magnitude is  $0.5/(-2 - M_V)$  and the error in the colour is the same for a given star. We also assumed full completeness for the sake of simplicity and this approach is used in the three later synthetic populations as well. We then created a population of 200 stars from this probability density function by applying the rejection method. The approximate limit of detection

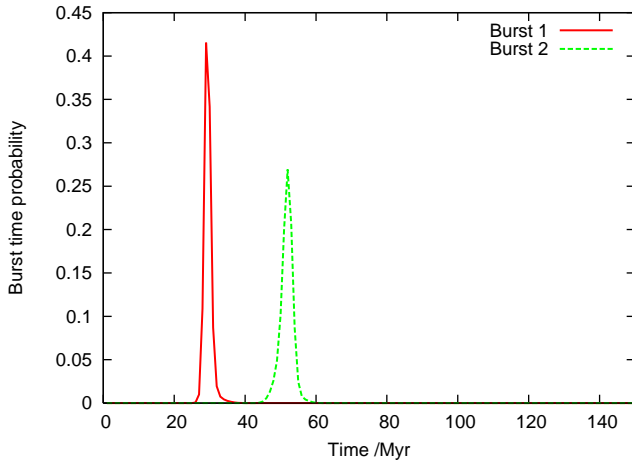


**Figure 3.** The posterior probabilities of the times of Population 1.

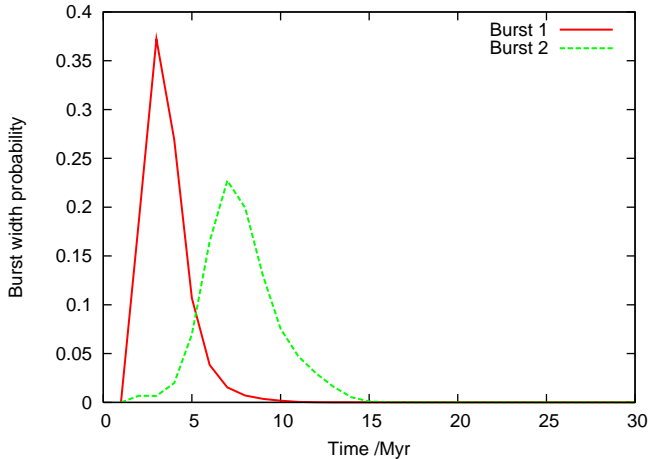


**Figure 4.** The posterior probabilities of the widths of Population 1.

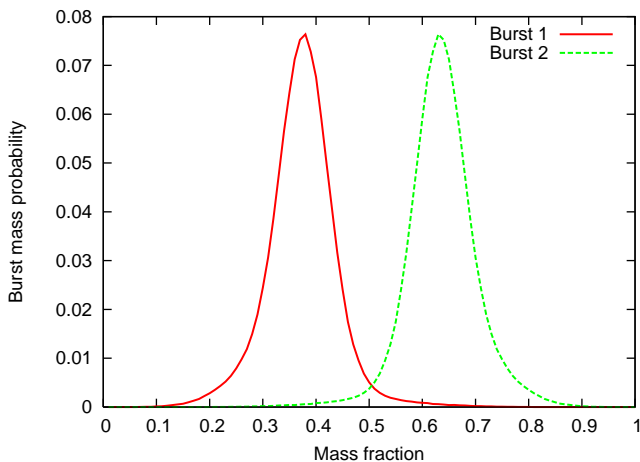


**Figure 5.** The posterior probabilities of the mass fractions of Population 1.

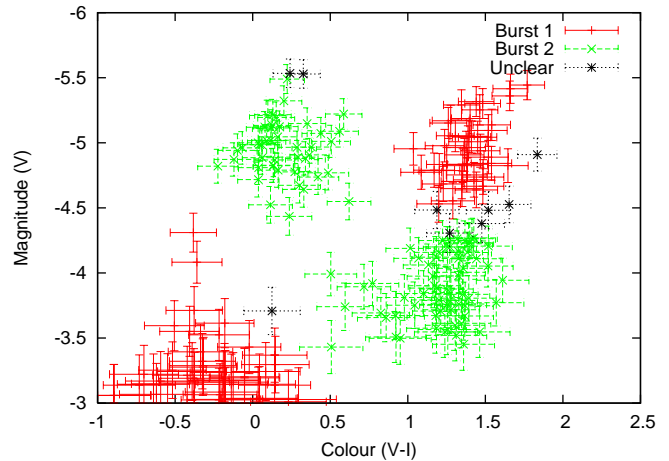


**Figure 6.** The CMD with classified stars of Population 1.

**Table 1.** The input parameters of Population 1.

Burst	Time /Myr	Width /Myr	Mass fraction
1	30	4	0.4
2	50	8	0.6

set by the stellar models is 300 Myr; stars older than this are either dead or below the magnitude cut-off

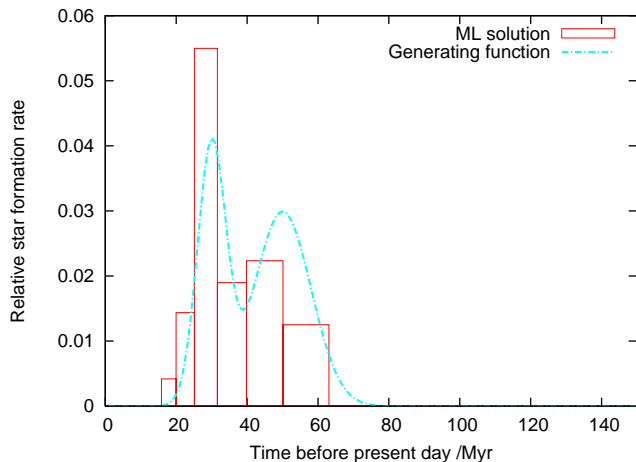
We ran the MCMC code and found that, as expected, the star formation history is best fitted with two bursts (Fig. 1). The modal values of the probability density function of the rate (Fig. 2) are a reasonable match for the generating function. The mean rate is very similar to the mode and the probability density functions for the rates are approximately normal. The probability density functions for the times, widths and masses are shown in Fig. 3, Fig. 4 and Fig. 5 respectively. Finally we present the CMD with the stars labelled according to their classification probabilities (Fig. 6). The first burst has produced the main sequence turn-off and the brighter red supergiants, the second has produced the dimmer red supergiants and the helium-burning stars on the blue loop.

If we consider the probability density functions of the parameters we see that they are unimodal and reasonably normal in appearance. We adopt the mode as our best estimate and present them together with the minimal 68 per cent credible intervals in Table 2. Happily they are in agreement with the input parameters. It is notable that the percentage error in the times is less than that of the masses and widths. To some extent there is a degeneracy in the latter two parameters: the star formation rate at the centre of the Gaussian can be reduced by either increasing the width or reducing the mass. We note that, unsurprisingly, if the number of stars is increased the uncertainties and the differences between the estimates and the input parameters are reduced. With  $10^4$  stars these become less than 1 Myr for the times and widths and 0.01 for the mass fractions.

By way of contrast we also provide the star formation history obtained by maximising  $\mathcal{L}_2$  with partial model CMDs that were binned according to advances of 0.1 in the base 10 logarithm of time. This histogram-based method is

**Table 2.** The estimated parameters of Population 1.

Burst	Time /Myr	Width /Myr	Mass fraction
1	$28^{+2}_{-1}$	$2^{+2}_{-1}$	$0.37^{+0.05}_{-0.05}$
2	$51^{+1}_{-2}$	$6^{+3}_{-1}$	$0.62^{+0.05}_{-0.05}$

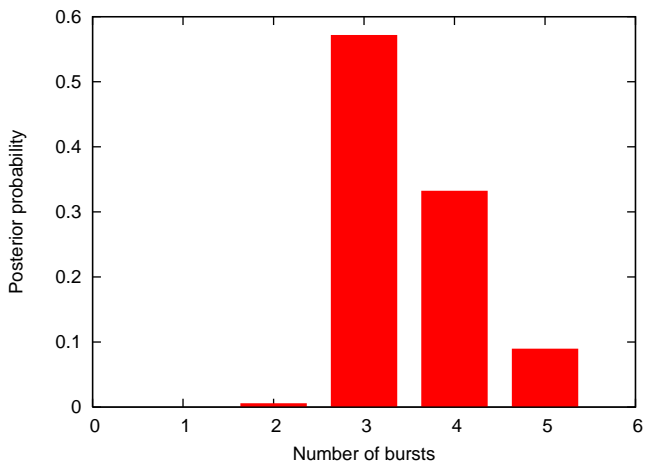
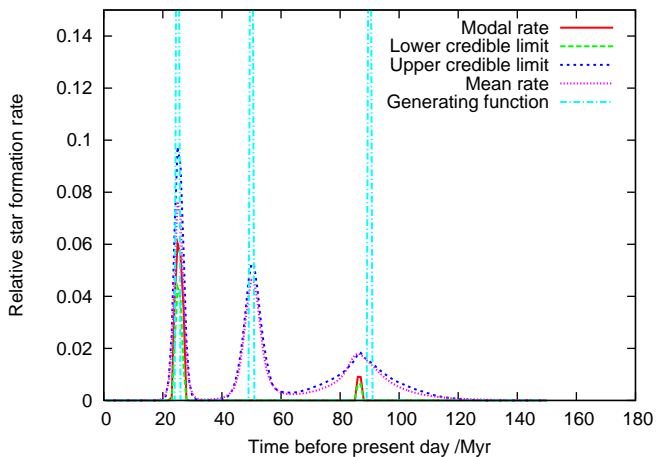
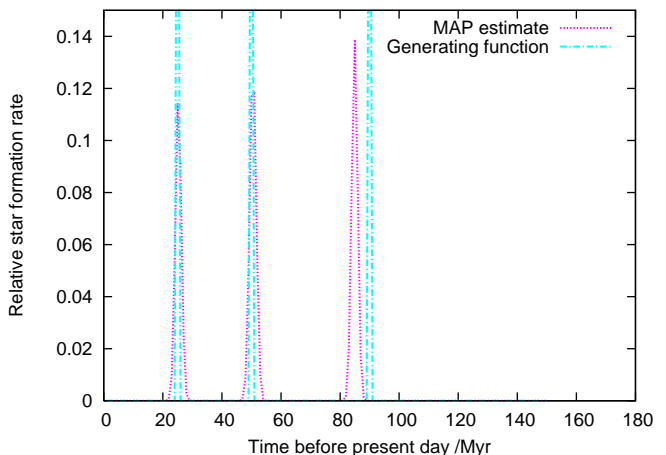

**Figure 7.** The histogram-based maximum likelihood ( $\mathcal{L}_2$ ) star formation history of Population 1.

the same as that of Dolphin (2002); the only difference is that we maximise the unbinned integrated likelihood  $\mathcal{L}_2$ , the same likelihood used in our Bayesian method, instead of the binned Poisson likelihood  $\chi^2_\lambda$ . To effect the maximisation we used a simple simulated annealing algorithm and the result is shown in Fig. 7. The match is reasonable but the shortcomings of the method are apparent: it is unable to fit a continuous function or to automatically identify the existence of two different components.

## 5.2 Population 2: Three delta-functions

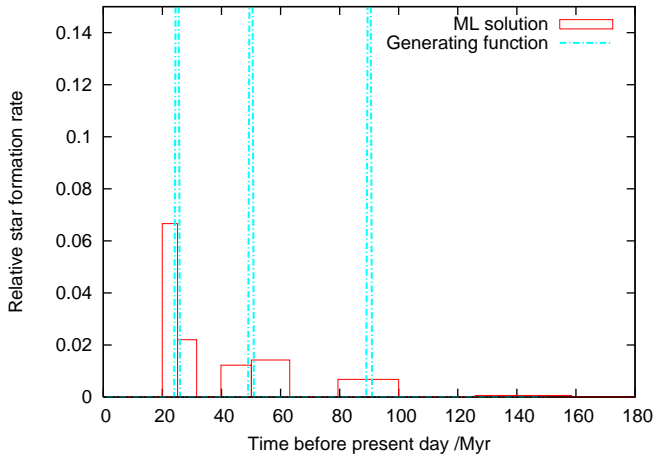
Three delta-function bursts provided our second test case. We used a star formation history consisting of delta-functions at 25, 50 and 90 Myr and generated 150 stars. We found, as expected, that three bursts provide the best fit (Fig. 8). The inferred parameters are given in Table 3 and the rate is shown in Fig. 9.

The modal rate is zero for much of the plot. This is a consequence of the fact that the MCMC samples consist of very narrow bursts. The posterior distribution of the rate at a given time thus has most of the probability at zero, with the rest at very high values corresponding to the occasional presence of a narrow burst. This highly-non normal distribution is difficult to represent adequately with the summary statistics plot. We therefore also present the maximum a posteriori (MAP) solution, which in this case is a much better indication of the nature of the generating function (Fig. 10). The bursts all have the minimum possible width of 1 Myr and would have been narrower still if the program had allowed it. In general the MAP estimate is an extreme and unrepresentative case but with this example the generating function is extreme as well. Random draw-


**Figure 8.** The posterior probabilities of the number of bursts used to fit Population 2. Three bursts give the best fit.

**Figure 9.** The inferred star formation history of Population 2. The posterior probability of the star formation rate at each point in time is summarised by its mean, mode and minimum 68 per cent credible interval.

**Figure 10.** The maximum a posteriori (MAP) star formation history of Population 2.

**Table 3.** The estimated parameters of Population 2.

Burst	Time /Myr	Width /Myr	Mass fraction
1	$25_{-1}^{+1}$	$1_{-1}^{+1}$	$0.28_{-0.03}^{+0.05}$
2	$50_{-2}^{+1}$	$1_{-1}^{+1}$	$0.33_{-0.06}^{+0.05}$
3	$85_{-2}^{+5}$	$1_{-1}^{+12}$	$0.36_{-0.05}^{+0.06}$

**Figure 11.** The histogram-based maximum likelihood ( $\mathcal{L}_2$ ) star formation history of Population 2.

ings from the posterior distribution are in most cases similar to this but with some scatter in the times and the masses.

If we consider the burst parameters we find that, within the uncertainties, the times are correctly identified and the masses are equal. The uncertainties in the times and the widths are highest for the oldest burst. This is a consequence of the fact that stellar populations change more slowly with increased time and hence their resolving power is weaker. The older stars are also dimmer and thus have bigger photometric errors.

As before we also provide the histogram solution (Fig. 11). The three bursts are identified, the times are correct and the relative allocation of star formation appears approximately equal. However, the increasing size of the temporal bins means that the rate is depicted as declining. The delta-function nature of the bursts is impossible to ascertain.

### 5.3 Population 3: A more complicated history

Hitherto we considered populations where the individual Gaussians had some physical meaning, that is, they corresponded to different bursts/events. We now present a star formation history where the Gaussians are only considered to be a useful parametrisation. Choosing the number of Gaussians is then not so much a matter of identifying different populations as selecting the appropriate number of parameters with which to fit the star formation history.

We chose a piecewise continuous functional form  $r(t)$  as the star formation history,

$$r(t) \propto t^2, \quad 0 < t < 40, \quad (37)$$

$$\propto t^{-1}, \quad 40 < t < 100, \quad (38)$$

$$\propto -At^2 + Bt - C, \quad 100 < t < 150, \quad (39)$$

where  $t$  has units of Myr,  $A = 32/25$ ,  $B = 1536/5$  and  $C = 17280$ . We generated 1000 stars from the CMD and applied the MCMC program. We found that three bursts are required for the best fit (Fig. 12) and that the inferred rate is a reasonable match to the generating function (Fig. 13). The only difficulty lies in the proper reproduction of the sharp peak at 40 Myr.

The histogram fit is shown in Fig. 14 and makes a poor contrast. The overall form is correct but the small bins at recent times have high uncertainties. A better match would probably be obtained by using fewer time bins.

### 5.4 Population 4: Direct model comparison with a flat star formation history

We finally considered a flat star formation rate out to 80 Myr. The Gaussians are very poorly-adapted to fitting such a history and a rectangular function would be far more appropriate. We demonstrated the power of the Reversible Jump approach by adding a fourth MCMC move, jumping between Gaussians and rectangular functions. For the latter, the time of a rectangle is that of its centre and the equivalent of the Gaussian standard deviation is the half-width.

We generated 2,000 stars and found that three bursts gave the best fit in the Gaussian case but that the rate is a poor match (Fig. 15), even with this abundance of data. The abrupt discontinuity at 80 Myr seems to have provoked a spike analogous to the Gibbs phenomenon found when a discontinuity is fitted with a Fourier series. By contrast one rectangle provides a far better match (Fig. 16). The posterior probabilities of the different models are in favour of the rectangles by a ratio of over a thousand to one.

The histogram fit is shown in Fig. 17 and is surprisingly poor. The logarithmic nature of the bins means that they become very small for times more recent than 10 Myr, even though we increased the bin size to 0.2 in the logarithm of time. This means that very small intervals of star formation are being fitted. These intervals can only be distinguished by the very small number of very rapidly-evolving massive stars and so the potential for uncertainty is high.

## 6 APPLICATION TO DATA

We applied our method to NGC 1313-F3-1, a young star cluster that forms part of a set of seven for which Larsen et al. (2011) were able to recover resolved stellar populations. This intriguing object shows evidence for two distinct bursts of recent star formation and is an excellent test subject for our new method. We first performed the analysis with  $V - I$  against  $V$  and with  $B - V$  against  $V$ . We then used the full data cube and compared our results and the inferred parameters are listed in Table 4.

Larsen et al. (2011) investigated the star formation history of NGC 1313-F3-1 with the CMD-fitting code FITSFH (Silva-Villa & Larsen 2010), which maximises the Poisson likelihood in the same way as Dolphin (2002). Their findings are shown in Fig. 18.

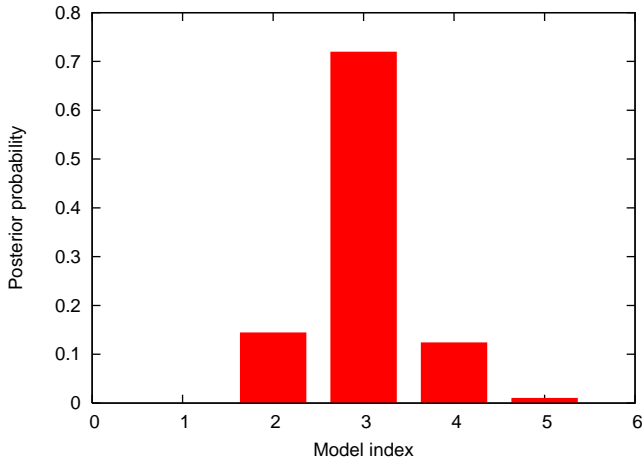


**Figure 12.** The posterior probabilities of the number of bursts used to fit Population 3. Three bursts give the best fit.

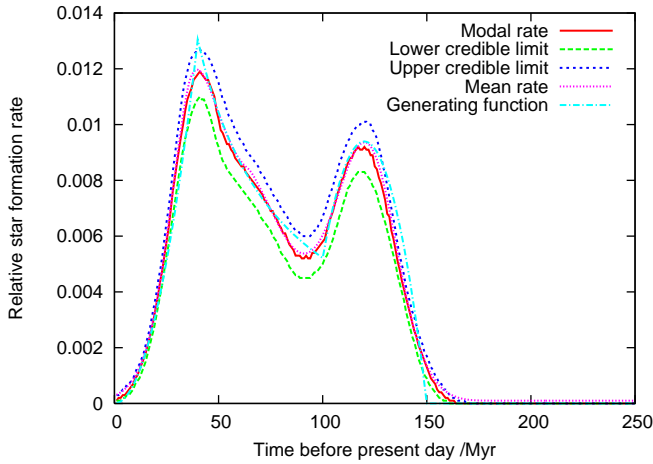


**Figure 13.** The inferred star formation history of Population 3. The posterior probability of the star formation rate at each point in time is summarised by its mean, mode and minimum 68 per cent credible interval

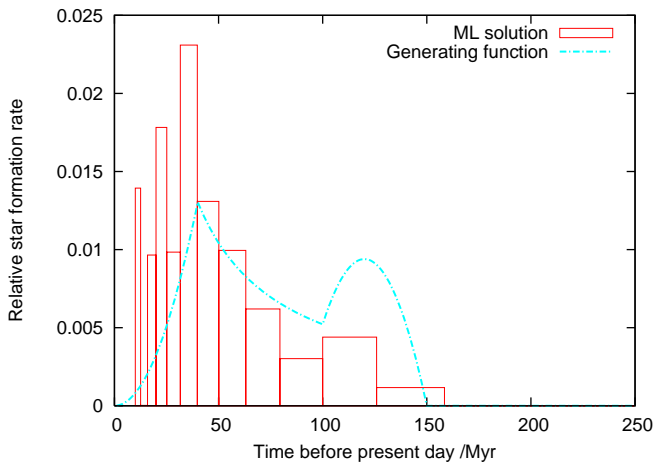


**Figure 14.** The histogram-based maximum likelihood ( $\mathcal{L}_2$ ) star formation history of Population 3.

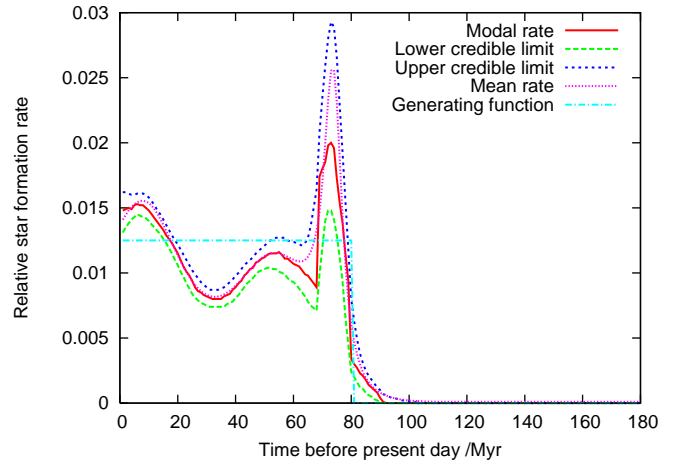


**Figure 15.** The inferred star formation history of Population 4 with Gaussians.

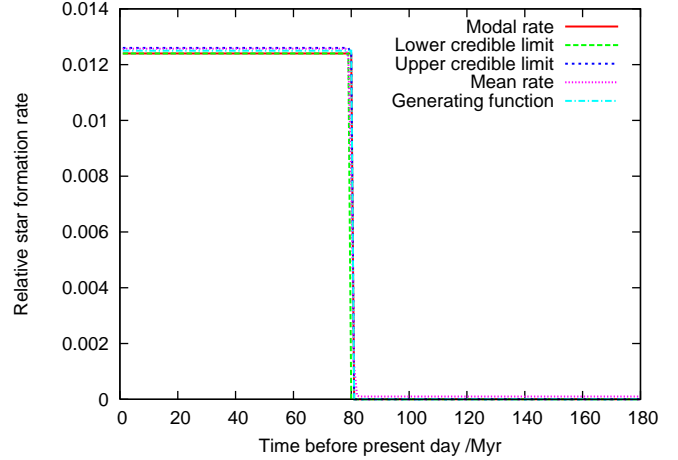


**Figure 16.** The inferred star formation history of Population 4 with one rectangle. The errors are almost invisible.

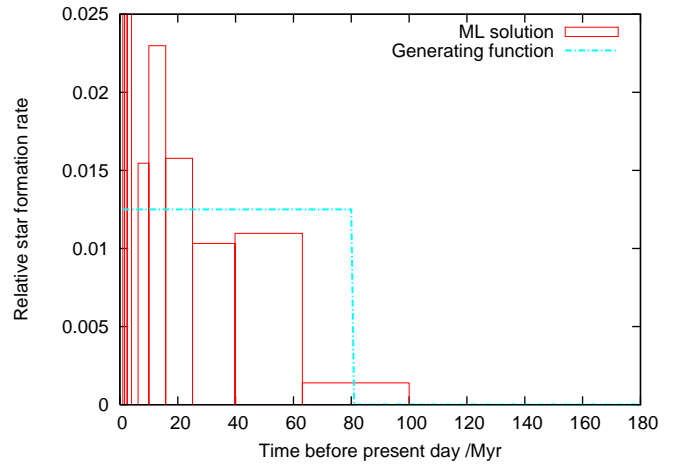


**Figure 17.** The histogram-based maximum likelihood ( $\mathcal{L}_2$ ) star formation history of Population 4.

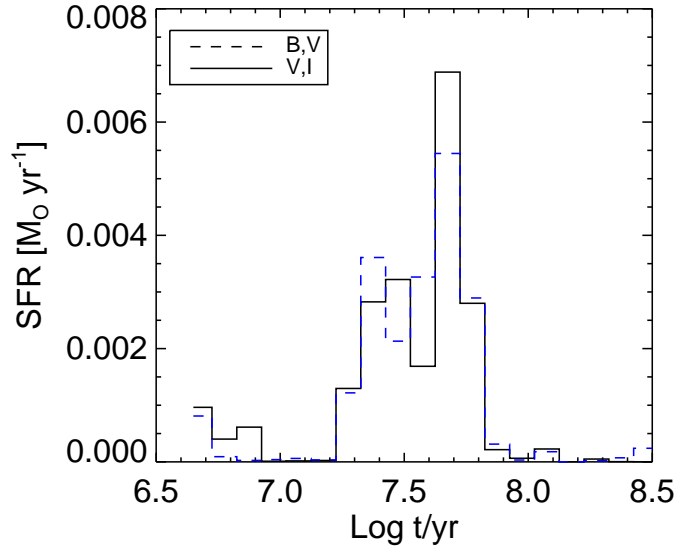


**Figure 18.** The Larsen et al. (2011) star formation history for NGC 1313-F3-1.

### 6.1 NGC 1313-F3-1 in two filters: V and V-I

We applied a magnitude cut in  $V$  at  $-3$  and thus adopted the completeness limits given in Larsen et al. (2011). This reduced the number of stars under consideration to 122. We found that three Gaussians provided the best fit (Fig. 19) and the rate is shown in Fig. 20. Two of the Gaussians are distinct and narrow bursts with well-defined times (Fig. 21) but the third is a very broad and ill-defined entity. It may represent a continuous rate of low-level star formation; alternatively it could be present to fit stars that, because of errors in the data and inadequacies in the models, are not accounted for by the more recent bursts.

We found that the most recently-formed stars, as identified by the classification probabilities in Fig. 22, appear to form a distinct group according to their spatial locations (Fig. 23). This could be evidence for a distinct and recently-formed population and is an unexpected bonus. Kinematic data would help test this theory but unfortunately it is not available.

We repeated the analysis but with the likelihood calculated by the Voronoi Tessellation error-blurring method ( $\mathcal{L}_1$ , from Section 2.4). The rate plot is shown in Fig. 24 and is very similar to its counterpart (Fig. 20).

### 6.2 NGC 1313-F3-1 in two filters: V and B-V

We applied the same magnitude cut as before and on this occasion found that two bursts provided the best fit (Fig. 25). The star formation history is shown in Fig. 26. The earlier burst at  $t_2 = 39_{-1}^{+1}$  Myr is well defined (Fig. 27) and matches its counterpart from the  $V-I$  analysis. The most recent event is much more nebulously defined and the very broad third burst is conspicuous by its absence.

### 6.3 NGC 1313-F3-1 in three filters

We finally construct the colour-colour-magnitude cube in  $B-V$ ,  $V-I$  and  $V$  and compare with the data. We find that

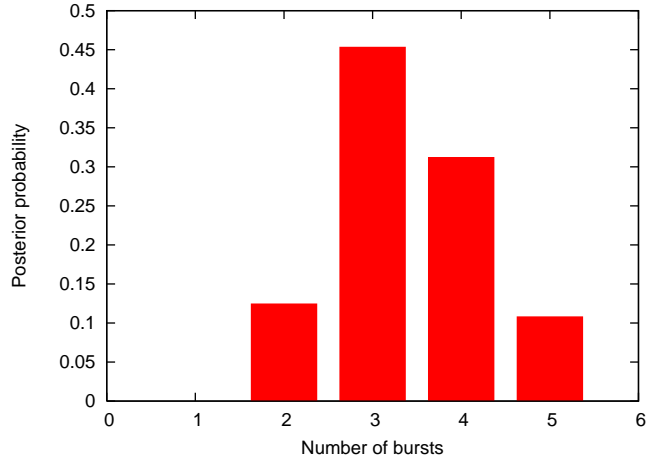


**Figure 19.** The posterior probabilities of the number of bursts used to fit NGC 1313-F3-1 when  $V$  and  $V-I$  are used. Three bursts give the best fit.

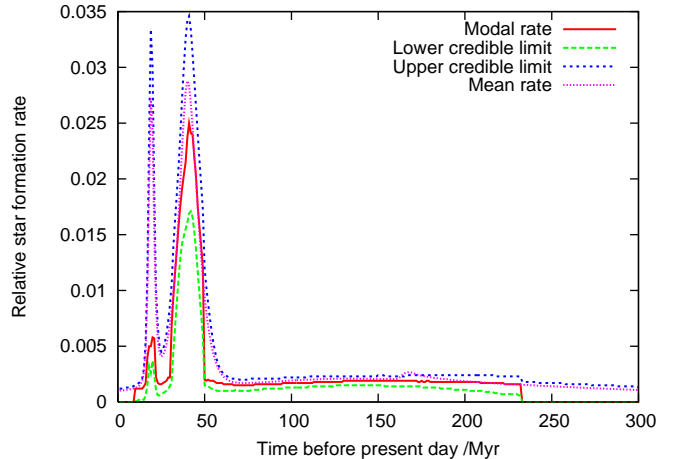


**Figure 20.** The inferred star formation history of NGC 1313-F3-1 when  $V$  and  $V-I$  are used. The posterior probability of the star formation rate at each point in time is summarised by its mean, mode and minimum 68 per cent credible interval.

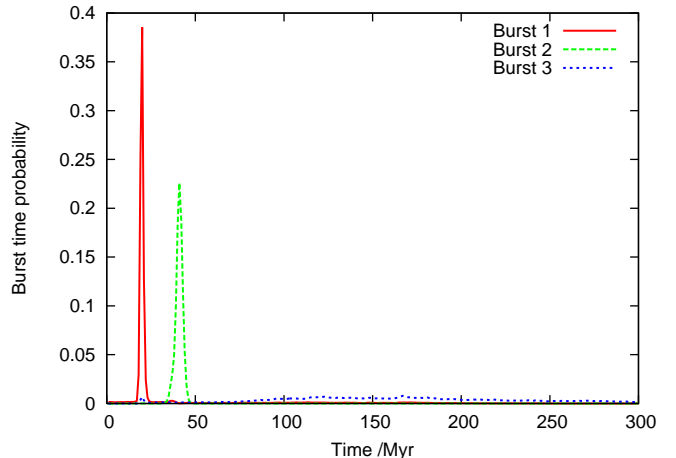


**Figure 21.** The posterior probabilities of the times of NGC 1313-F3-1 with  $V$  and  $V-I$ .

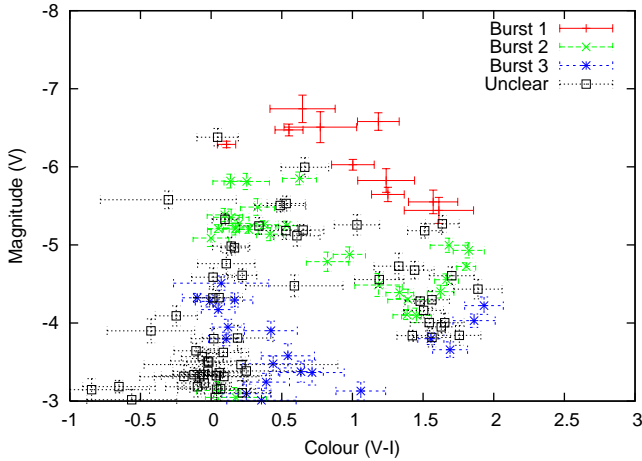


**Figure 22.** The CMD with classified stars of NGC 1313-F3-1 with  $V$  and  $V - I$ .

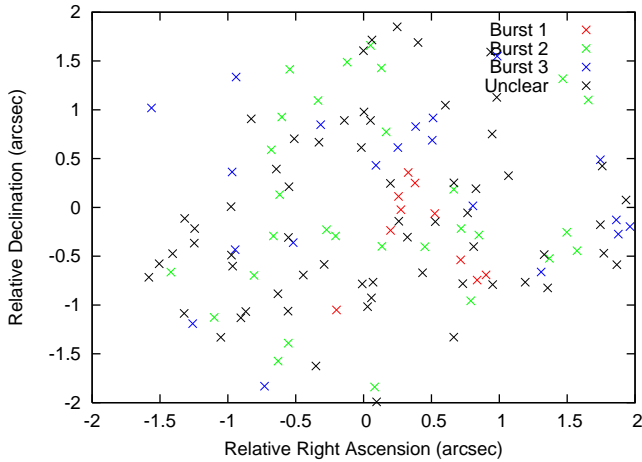


**Figure 23.** The spatial locations of the classified stars of NGC 1313-F3-1 with  $V$  and  $V - I$ . Those from Burst 1 appear to form a group.

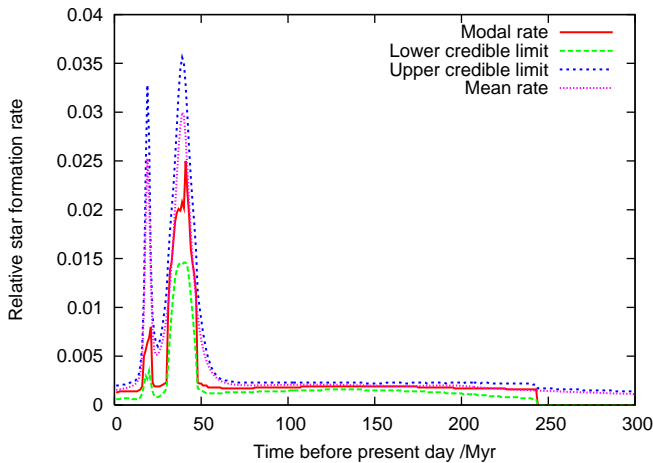


**Figure 24.** The inferred star formation history of NGC 1313-F3-1 with  $\mathcal{L}_1$  as the likelihood when  $V$  and  $V - I$  are used.

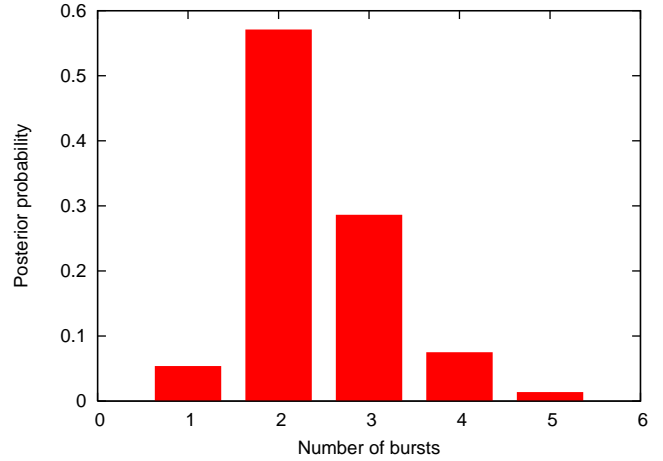


**Figure 25.** The posterior probabilities of the number of bursts used to fit NGC 1313-F3-1 when  $V$  and  $B - V$  are used. Two bursts give the best fit.

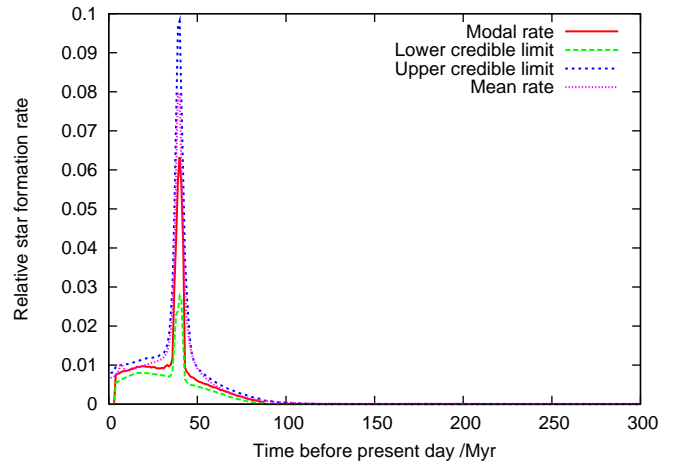


**Figure 26.** The inferred star formation history of NGC 1313-F3-1 when  $V$  and  $B - V$  are used. The posterior probability of the star formation rate at each point in time is summarised by its mean, mode and minimum 68 per cent credible interval.

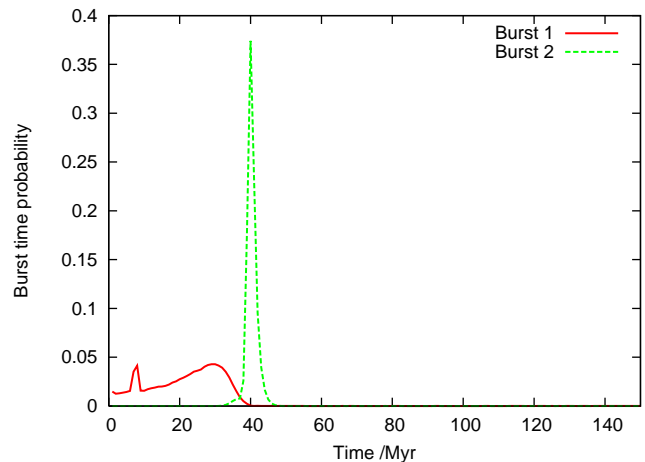


**Figure 27.** The posterior probabilities of the times of NGC 1313-F3-1 with  $V$  and  $B - V$ .

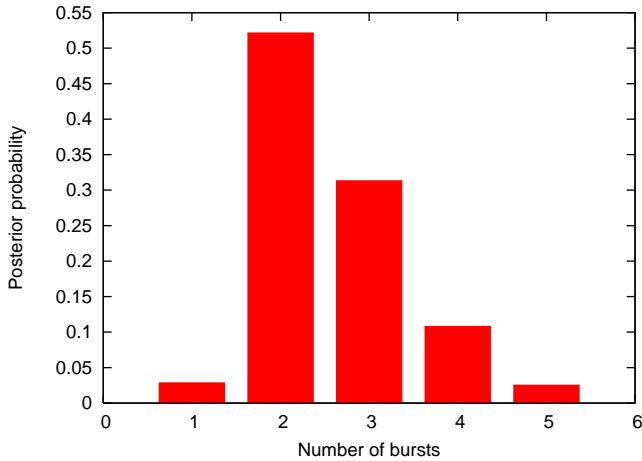


**Figure 28.** The posterior probabilities of the number of bursts used to fit NGC 1313-F3-1. Two bursts give the best fit but there is reasonable support for three and so we consider both models.

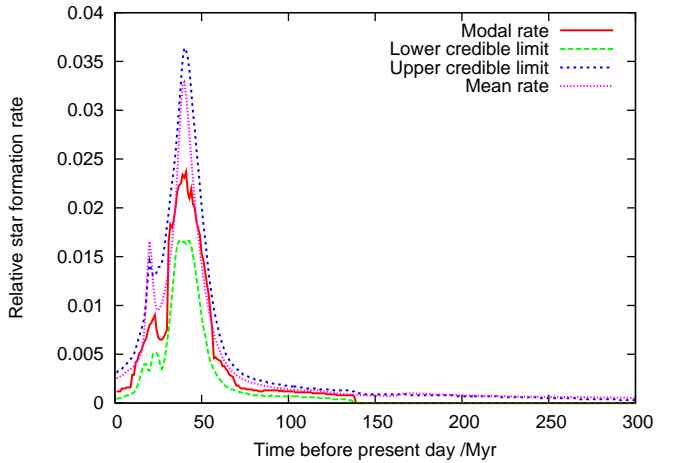


**Figure 30.** The three burst inferred star formation history of NGC 1313-F3-1 when all the colours are used.

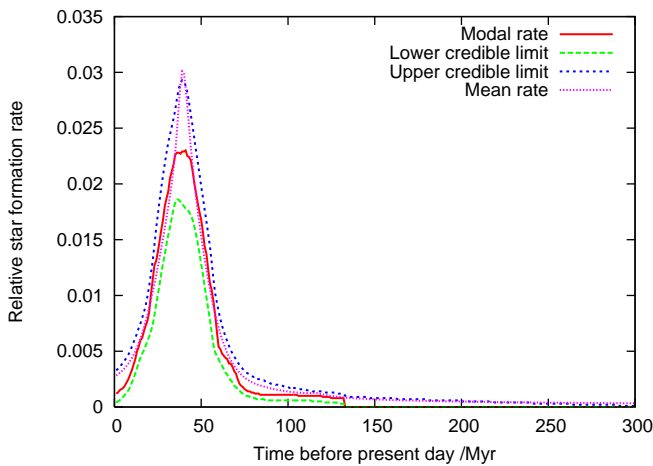


**Figure 29.** The two burst inferred star formation history of NGC 1313-F3-1 when all the colours are used. The posterior probability of the star formation rate at each point in time is summarised by its mean, mode and minimum 68 per cent credible interval.

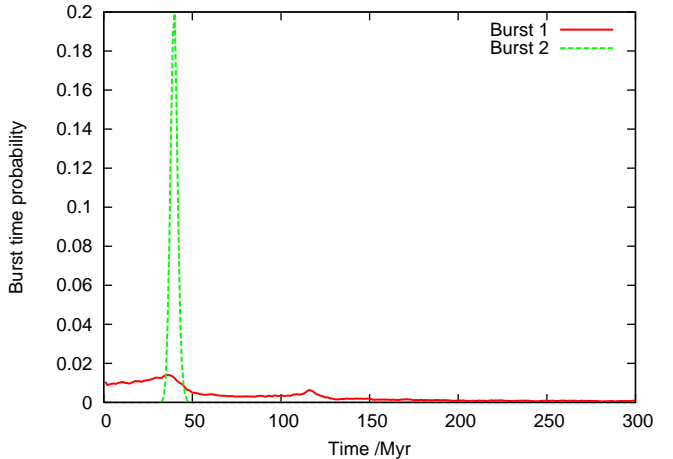


**Figure 31.** The two burst posterior probabilities of the times of NGC 1313-F3-1 when all the colours are used.

the most probable number of Gaussians is two (Fig. 25) but that there is reasonable posterior support for three bursts.

We plot the rate with two (Fig. 29) and three (Fig. 30) bursts and similarly the plot of the marginal probabilities of the times (Fig. 31 and Fig. 32). The earlier burst is amorphous enough that we may doubt its existence and ascribe it perhaps to uncertainties in the model. Alternatively such uncertainties could be the reason why the detection is not strong enough. This analysis demonstrates that to infer the star formation history of a resolved stellar population one must consider the probabilities of different scenarios rather than optimise some fitting function.

## 7 CONCLUSIONS

We have demonstrated a new technique to infer the star formation histories of stellar populations. Our Gaussian parametrisation is a reasonable way of ensuring a continuous

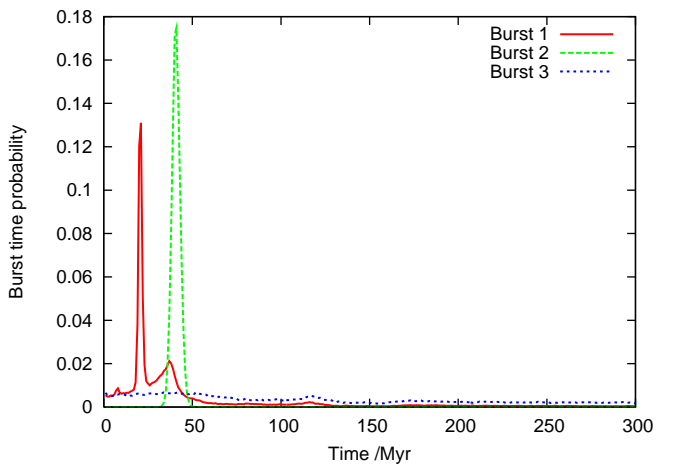


**Figure 32.** The three burst posterior probabilities of the times of NGC 1313-F3-1 when all the colours are used.

**Table 4.** The estimated parameters of NGC 1313-F3-1.

Burst	Time /Myr	Width /Myr	Mass fraction
V and V – I fitted with three bursts.			
1	$19^{+1}_{-1}$	$1^{+1}_{-1}$	$0.1^{+0.06}_{-0.03}$
2	$40^{+2}_{-1}$	$5^{+3}_{-2}$	$0.39^{+0.1}_{-0.08}$
3	$166^{+54}_{-78}$	$1^{+144}_{-1}$	$0.47^{+0.11}_{-0.12}$
V and B – V fitted with two bursts.			
1	$29^{+5}_{-16}$	$1^{+32}_{-1}$	$0.58^{+0.10}_{-0.10}$
2	$39^{+1}_{-1}$	$1^{+2}_{-1}$	$0.41^{+0.10}_{-0.10}$
V, V – I and B – V fitted with two bursts.			
1	$39^{+1}_{-2}$	$13^{+3}_{-5}$	$0.74^{+0.16}_{-0.21}$
2	$35^{+57}_{-35}$	$1^{+120}_{-1}$	$0.25^{+0.21}_{-0.16}$
V, V – I and B – V fitted with three bursts.			
1	$20^{+23}_{-7}$	$1^{+31}_{-1}$	$0.13^{+0.15}_{-0.13}$
2	$40^{+2}_{-2}$	$3^{+6}_{-2}$	$0.50^{+0.18}_{-0.16}$
3	$451^{+111}_{-51}$	$1^{+126}_{-1}$	$0.25^{+0.10}_{-0.20}$

function of time. The use of Reversal Jump MCMC means that we can automatically apply Occam’s Razor and find the number of Gaussians most appropriate for modelling the data, thus avoiding overfitting. The Reversible Jump process also allows the direct comparison of differently-parametrised models.

We note that it is possible to apply transdimensional Bayesian methods to the traditional histogram parametrisation. The principal difficulty would lie in the calculation of the Jacobian of the transformation between  $M$  time bins and, for example,  $M+1$ . We maintain though that the Gaussian burst parametrisation is preferable. In the case when the population really consists of distinct bursts then the advantages of our method are obvious because we can infer the parameters of the bursts. We can also infer the classification probabilities that a given star was formed in a given burst.

Our method could also be easily adapted to fit the parameters used in stellar models by making them into variables along with the star formation history. With an appropriate prior one could then recover the posterior probability distribution for the parameter given the data under consideration. Naturally only very high quality data would be suitable for this process and it would be wise to compare several different data sets.

We are aware that we have been somewhat cavalier with the treatment of errors and that a better approach would take into account incompleteness as a function of magnitude, blending and model uncertainties. The first of these could be addressed by the inclusion of a parametrised form of the completeness function with appropriate priors. A sigmoid between full and zero completeness with a location parameter and a scale parameter is one possibility. These parameters would then be varied in the MCMC process. One could similarly fit the overall extinction and the distance modulus if these were poorly-constrained.

More general improvements are also possible. The prior probabilities for the masses and the widths could perhaps be improved by the consideration of the behaviour of real

star formation bursts. Alternatively the priors could be parametrised and hyperpriors placed on the parameters. An example of this would be to allow  $\alpha$ , the concentration parameter of the symmetric Dirichlet distribution, to vary in the MCMC process but with a hyperprior that favoured  $\alpha = 1$  over  $\alpha = 100$  or  $\alpha = 0.01$ . This approach is probably a better way of representing our ignorance (Stephens 2000a). The use of Gaussians is of course entirely arbitrary and we are ready to believe that other parametrisations may be more physically motivated and offer better fits. We compared exponentials with Gaussians and found that the latter was favoured by about three to one in the posterior probabilities; nevertheless there may be other stellar populations where this is not true. In the future it may be sensible to compare more general symmetric and asymmetric functions.

## ACKNOWLEDGEMENTS

We thank the reviewer for many useful suggestions and Christopher Berry for suggesting exponentials as an alternative parametrisation. JJW was supported by a stipend from STFC, though sadly this is no longer the case. Fig. 18 is from Larsen et al. (2011) and is reproduced with permission from Astronomy & Astrophysics, ©ESO.

## REFERENCES

- Akaike H., 1974, *IEEE Transactions on Automatic Control*, 19, 716723
- Aparicio A., Hidalgo S. L., 2009, *AJ*, 138, 558
- Böhm-Vitense E., 1958, *ZAp*, 46, 108
- Brewer B. J., Pártay L. B., Csányi G., 2011, *Statistics and Computing*, 21, 649
- de Jager C., Nieuwenhuijzen H., van der Hucht K. A., 1988, *A&As*, 72, 259
- Denoeux T., 2013, *IEEE Transactions on Knowledge and Data Engineering*, 25, 119
- Dolphin A., 1997, *New Astronomy*, 2, 397
- Dolphin A. E., 2002, *MNRAS*, 332, 91
- Eggleton P. P., 1971, *MNRAS*, 151, 351
- Eldridge J. J., Izzard R. G., Tout C. A., 2008, *MNRAS*, 384, 1109
- Eldridge J. J., Vink J. S., 2006, *A&A*, 452, 295
- Green P. J., 1995, *Biometrika*, 82, 711
- Hastings W. K., 1970, *Biometrika*, 57, 97
- Hauschild T., Jentschel M., 2001, *Nuclear Instruments and Methods in Physics Research A*, 457, 384
- Jasra A., Holmes C. C., A. S. D., 2005, *Statistical Science*, 20, 5067
- Jeffreys H., 1939, *Theory of Probability*. Oxford Univ. Press
- , 1946, *Royal Society of London Proceedings Series A2*, 214, 453
- Jegerlehner B., Neubig F., Raffelt G., 1996, *Phys. Rev. D*, 54, 1194
- Jørgensen B. R., Lindegren L., 2005a, in *ESA Special Publication*, Vol. 576, *The Three-Dimensional Universe with Gaia*, Turon C., O’Flaherty K. S., Perryman M. A. C., eds., p. 171
- , 2005b, *A&A*, 436, 127

- Kauffmann G., Heckman T. M., White S. D. M., Charlot S., Tremonti C., Brinchmann J., Bruzual G., Peng E. W., Seibert M., Bernardi M., Blanton M., Brinkmann J., Castander F., Csábai I., Fukugita M., Ivezić Z., Munn J. A., Nichol R. C., Padmanabhan N., Thakar A. R., Weinberg D. H., York D., 2003, *MNRAS*, 341, 33
- Larsen S. S., de Mink S. E., Eldridge J. J., Langer N., Bastian N., Seth A., Smith L. J., Brodie J., Efremov Y. N., 2011, *A&A*, 532, A147
- Marin J. M., Mengersen K. L., P. R. C., 2005, *Handbook of Statistics*, 25
- Mauron N., Josselin E., 2011, *A&A*, 526, A156+
- Mighell K. J., 1999, *ApJ*, 518, 380
- Naylor T., 2009, *MNRAS*, 399, 432
- Naylor T., Jeffries R. D., 2006, *MNRAS*, 373, 1251
- Nugis T., Lamers H. J. G. L. M., 2000, *A&A*, 360, 227
- Press W. H., Teukolsky S. A., Vetterling W. T., Flannery B. P., 1992, *Numerical Recipes in Fortran: The Art of Scientific Computing*, 2nd edn. Cambridge Univ. Press
- Richardson S., Green P. J., 1997, *J. R. Statist. Soc Ser. B*, 59, 731
- Schwarz G. E., 1978, *Annals of Statistics*, 6, 461464
- Silva-Villa E., Larsen S. S., 2010, *A&A*, 516, A10
- Small E. E., Bersier D., Salaris M., 2013, *MNRAS*, 428, 763
- Stancliffe R. J., Eldridge J. J., 2009, *MNRAS*, 396, 1699
- Stephens M., 2000a, *The Annals of Statistics*, 28, 40
- , 2000b, *J. R. Statist. Soc Ser. B*, 62, 795
- Tolstoy E., Saha A., 1996, *ApJ*, 462, 672
- Vink J. S., de Koter A., Lamers H. J. G. L. M., 2001, *A&A*, 369, 574
- von Hippel T., Jefferys W. H., Scott J., Stein N., Winget D. E., De Gennaro S., Dam A., Jeffery E., 2006, *ApJ*, 645, 1436
- Weisz D. R., Dalcanton J. J., Williams B. F., Gilbert K. M., Skillman E. D., Seth A. C., Dolphin A. E., McQuinn K. B. W., Gogarten S. M., Holtzman J., Rosema K., Cole A., Karachentsev I. D., Zaritsky D., 2011, *ApJ*, 739, 5
- Westera P., Lejeune T., Buser R., Cuisinier F., Bruzual G., 2002, *A&A*, 381, 524

